Proceedings Paper:
Karlsen, J., Dennis, A. and Rigby, S. orcid.org/0000-0001-6844-3797 (2025) The inception of a rapid predictor for blast wave shielding: thinking radi(c)ally. In: Syngellakis, S. and Teixeira-Dias, F., (eds.) WIT Transactions on The Built Environment. 17th International Conference on Structures under Shock and Impact (SUSI 2025), 09-11 Jun 2025, Edinburgh, UK. WIT Press , pp. 85-96. ISBN: 9781784664954 ISSN: 1743-3509 EISSN: 1743-3509

https://doi.org/10.2495/SUSI250081

THE INCEPTION OF A RAPID PREDICTOR FOR BLAST WAVE SHIELDING: THINKING RADI(C)ALLY

JAY KARLSEN[1], ADAM A. DENNIS[1] & SAMUEL E. RIGBY[1,2]
[1]School of Mechanical, Aerospace & Civil Engineering, University of Sheffield, Sheffield, UK
[2]Arup Resilience, Security & Risk, Manchester, UK

ABSTRACT

A rapid and accurate predictor of blast effects in a geometrically complex urban environment has considerable practical value. Therefore, it is imperative to understand the behaviours that arise from blast–obstacle interaction; in particular the 'primary' behaviours, like shielding and channelling, which govern the magnitude and distribution of blast loading globally. However, these are entangled with highly-localised, second-order behaviours, like clearing and incidence effects, whose sensitivity and non-linearity have impeded the development of a generalised, first-order predictor for the primary behaviours. Consequently, this work begins to decouple them to permit a study of shielding in isolation. It is demonstrated that many of these secondary effects stem from the mismatch in geometry between the curved blast wave and the flat faces of the rectilinear obstacles commonly studied. Therefore, by curving the obstacle to match the wavefront, a planar interaction is compelled at all stand-off distances, and these secondary behaviours are eliminated. With the effects of shielding isolated, a parametric study of 273 curved wall geometries is undertaken in *Viper::Blast*, varying the footprint dimensions of an infinitely tall, rigid structure, and its stand-off from a hemispherical surface charge. Full-field peak specific impulse is measured at ground level and the data is used to demonstrate a fundamental consistency in the distribution of the loading across the full extent of the shielded region. A conservative, reduced-order representation for the distribution of peak specific impulse within the shielded region is developed and it is shown to be generalisable for annular sector obstacles of any stand-off distance, size or scale. Future work shall leverage this in the development of a fast-running engineering model for the prediction of the blast loading in the wake of an obstacle.

Keywords: blast, shielding, blast–obstacle interaction, parametric, numerical modelling, polar.

1 BACKGROUND

Blast wave shielding is the behaviour that describes the mitigation of blast loading in the wake of an obstacle [1], [2]. Shielding can thus be leveraged by blast protection engineers [2] and, more generally, it (along with channelling) fundamentally dictates blast loading parameters in an urban environment [1]. Understanding, quantifying, and predicting the mechanisms involved in shielding is therefore of immense practical significance, and as a consequence, blast wave shielding has been extensively studied. There are many independent numerical and experimental investigations that parametrically explore the relationship between an obstacle's dimensions and peak pressure and impulse reduction, often relative to the unobstructed case (e.g., [3]–[9]). Obstacles are shown to have considerable mitigative effects, reducing peak pressure by up to 80% [4], [6], peak specific impulse by up 60% [4], and sustaining the loading reduction to significant distances behind the obstacle [2].

From these investigations, a diverse array of predictive tools have been produced for the estimation of the reduced loading caused by shielding. There are largely two loading cases for which there are predictors: the reflected loading on a structure protected by a leading obstacle (e.g., [3]–[6]), and the full-field incident effects in the wake of a lone obstacle (e.g., [7]–[10]). The latter is of particular interest herein, as estimating full-field conditions rapidly and accurately is a prerequisite to the post-blast inverse characterisation of explosive events,

WIT Transactions on The Built Environment, Vol 215, © 2025 WIT Press
www.witpress.com, ISSN 1743-3509 (on-line)
doi:10.2495/SUSI250081

which has implications for the coordination of emergency life-saving response efforts [11]. It is observed that, in all cases, these incident predictors are developed from datasets measured at an arbitrary lateral extent, e.g., measurements constrained to ground level loading, or elevations below the obstacle's height (or some multiple of it). However, the lateral extent of an obstacle's influence grows considerably with the distance behind it [12]. Consequently, none of these predictive methodologies can estimate the full extent of an obstacle's shielding, nor the magnitude and distribution of the loading between this boundary and the spatial limits of their measurements.

Therefore, this work seeks to expand on prior parametric studies to characterise the influence of an obstacle's dimensions and stand-off distance on its mitigation of blast loading. In particular, the full lateral extent of the shielded zone shall be identified, with the view to support its prediction in forthcoming work. Notably, the rectilinear blast wall, on which prior studies have focused, is posited to be somewhat limiting in the insight it offers into shielding as a fundamental blast–obstacle interaction behaviour. Consequently, an alternative geometry is adopted – that of an annular sector – to eliminate the interference of several second-order behaviours that otherwise superpose with shielding, distorting the measurable effects by an unquantifiable amount. It is shown that the shielded region, once its full extent is isolated, exhibits an extremely consistent pattern of behaviour, irrespective of the distance behind the obstacle at which the effects are measured, and irrespective of the dimensions, scale and stand-off distance of the obstacle. Finally, a physically rationalised, reduced-order model is developed for this consistent behavioural regime.

2 DESIGNING THE OBSTACLE

An investigation of fundamental blast–obstacle interaction behaviour reasonably necessitates the study of lone obstacles of relatively simple geometry. Published literature seemingly conforms with this as a rectilinear, planar blast wall (often of infinite length) is commonly employed in the study of shielding effects [3]–[9]. The simplicity of the rectilinear case may have been assured during the nuclear-scale investigations of the mid-twentieth century [2], when 'an atomic bomb [was] the most likely form of attack against surface structures' [13, p. 239]. Considering explosive yields on the order of kilotonnes and megatonnes [14], the planar shock assumption is approximately valid [15] and thus impingement on a rectilinear obstacle would be uniform and perfectly orthogonal. However, modern threats have net explosive quantities between three and six orders of magnitude lower [16], meaning the assumption of a planar shock ceases to be appropriate and a blast wave's curvature must be considered [2].

Fig. 1(a)–(d) illustratively contrasts the interaction of a planar and a curved blast wave with a rectilinear obstacle. In both cases, the mechanisms of reflection, clearing and shielding are present. These shall be termed 'primary' behaviours, as they are guaranteed to manifest from the interaction of a blast wave with any finitely sized obstacle. In the case of the curved wave's impingement, an array of additional 'secondary' behaviours arise from the geometric mismatch between the spherically expanding shock and the flat wall, e.g., variability in incident loading parameters across the obstacle's face due to differing stand-off distances point-to-point [17]; oblique reflection with variation in incident angle [10]; the potential for Mach reflection [14], [18]; local shielding in the shadow of the front corners [12], [13], [19]. These secondary behaviours produce unquantifiable interference with the flow-field, superposing with the shielding (and other primary behaviours) in a way that cannot be decoupled.

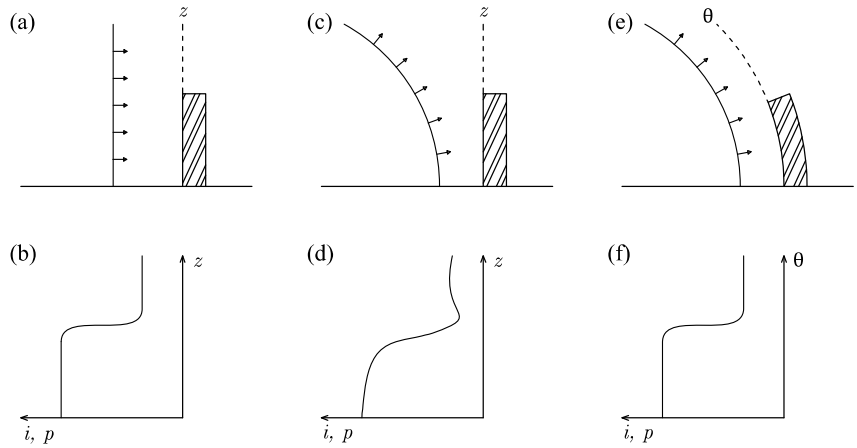

Figure 1: An illustrative contrast of planar and oblique blast–obstacle interaction. (a), (c) and (e) Radial cross-section through a blast wave's propagation; (b), (d) and (f) Representative peak specific impulse (i) and pressure (p) distribution along and beyond the reflecting plane for the scenarios depicted in (a), (c) and (e), respectively. Note the disrupting effects of the superposing secondary behaviours in (d) compared to planar interaction of (b) and (f).

Ultimately, the data-driven analysis of such a scenario is inappropriate when trying to understand any singular interaction behaviour. As such, despite the apparent simplicity of the rectilinear obstacle, an alternative geometric configuration is required to compel the manifestation of only the primary behaviours and thereby isolate 'pure' shielding.

A planar shock provides the necessary behavioural simplifications to enable a direct and isolated study of shielding, however its conventional representation is impractical to assume. Fig. 1(e) and (f) offers an alternative to this: rather than 'flattening' the shock to match the obstacle, the obstacle is instead curved to match the shock. In so doing, the analytical benefits of the planar shock assumption are obtained whilst guaranteeing physical validity for obstacles of any stand-off distance, size or scale.

The interacting geometry studied herein shall be annular sectors that match exactly the plan curvature of a free-field blast wave's spherical expansion. Using these, a data-driven, numerical investigation is undertaken to identify the extent of a single obstacle's shielding in the absence of localised, sensitive and interfering secondary behaviours.

3 MODELLING AND POST-PROCESSING

3.1 Parametric geometry

The magnitude and distribution of peak specific impulse in the wake of an obstacle is to be parametrically investigated with respect to the geometry of an annular sector. The variables considered are illustrated in Fig. 2 and defined below:

- Stand-off distance to rear face, R (m).
- Projected angle, θ (°), as a measure of lateral extent.
- Obstacle depth, d (m), measured radially.

The charge is a hemispherical ground burst (0.5 kg), and the longitudinal dimension of the obstacle is infinite – as is typical of prior investigations. Note, these two specifications permit the subsequent findings to be applicable to either a blast wall of infinite length or a building of infinite height.

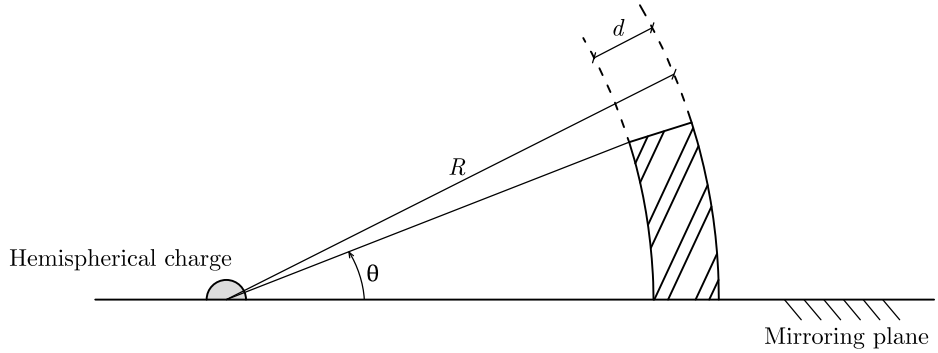

Figure 2: Plan elevation of the annular sector's geometry, with the parametric variables indicated.

The values sampled for each variable are as follows: R (m) = {4, 5, … 9, 10}; θ (°) = {10, 15, … 35, 40}; d (m) = {0.04, 0.2, 0.5, 1, 2, 3}.

To eliminate the potential for near-field blast–obstacle interaction and the associated complexities [20], variable combinations where the obstacle's front face stand-off distance is less than 3 m/kg$^{1/3}$ were neglected from the study, i.e., $R - d \geq 3$ m/kg$^{1/3}$. This reduces the number of unique geometry combinations available to study from 294 to 273.

3.2 Simulation set-up

Viper::Blast is a commercially available computational fluid dynamics software that '[predicts] blast loads on structures of non-trivial geometry' [21, p. 6]. Its predictive accuracy has been experimentally validated for blasts in both unobstructed and obstructed environments [21], [22], including cases of shielding [23]. Consequently, *Viper::Blast* is appropriate for use in the subsequent numerical investigation of shielding.

Beyond a scaled distance of 2 m/kg$^{1/3}$, the load predicted by both the isothermal burst and multi-material representations of a charge in *Viper::Blast* are shown to have converged [21]. Therefore, when modelling far-field interactions, the more computationally efficient isothermal burst method is commonly adopted [21]–[23]; this will be repeated herein.

Each geometric configuration is therefore simulated independently within *Viper::Blast*, importing the annular sector obstacle geometries as a triangulated surface mesh from a stereolithography file. The simulations leverage 1D to 3D remapping, and quarter symmetry about the ground plane and obstacle centreline to improve computational efficiency; eighth symmetry was considered, but interfering reflections from the fictitious second obstacle occurred with small values of R. All boundaries are therefore transmissive, besides the symmetry planes which are rigid reflecting. To produce the necessary 0.5 kg hemispherical ground burst, a unit mass sphere of TNT is initialised.

A polar arrangement of probes is used to record the spatial and temporal variation in pressure at ground level, at stand-off distances between 1 m and 15 m. The probes are radially

separated by two cell lengths and circumferentially separated by 1°. From these, peak specific impulse at each measurement point is approximated via numerical integration of the pressure–time history. It was confirmed for all obstacle geometries that a 70° arc of probes is sufficient to capture the full lateral extent of the shielded region.

Following a systematic domain study, as outlined by Chester et al. [23], it was confirmed that the dimensions of the domain are such that rarefaction waves from the ambient transmit boundaries arrive too late to interfere with the peak specific impulse, though a 2 m 'buffer' is required [22] (reducing the extent of the effective data collection zone to 13 m). A subsequent mesh refinement study identified sufficient convergence in peak specific impulse for unit cells of length 0.04 m.

3.3 Post-processing

Throughout, peak specific impulse is reported relative to the unobstructed case; $i_{p,r}$ is the measured specific impulse as a percentage proportion of the free-field value.

Fig. 3(a) depicts a spatial map of the post-processed relative peak specific impulse for a representative wall geometry. The colour map highlights three distinct and intuitive behavioural regions: relative enhancement, due to the front face reflection; relative reduction where the obstacle's redistribution of energy means that the loading is locally lessened; and a region of no significant change, where (beyond some distance) the obstacle causes the peak impulse to be no more or less severe than the unobstructed case. For clarity, Fig. 3(b) extracts the circumferential distribution of $i_{p,r}$ at the common radius highlighted in Fig. 3(a).

Herein, a point is considered 'shielded' if its relative peak specific impulse is 97.5% or less, i.e., the obstacle must reduce peak impulse by at least 2.5% from the free-field event. All data points that do not meet this criterion, e.g., the solid black lines in both Fig. 3(a) and (b), are then eliminated from consideration, as illustrated by the shaded region in Fig. 3(b).

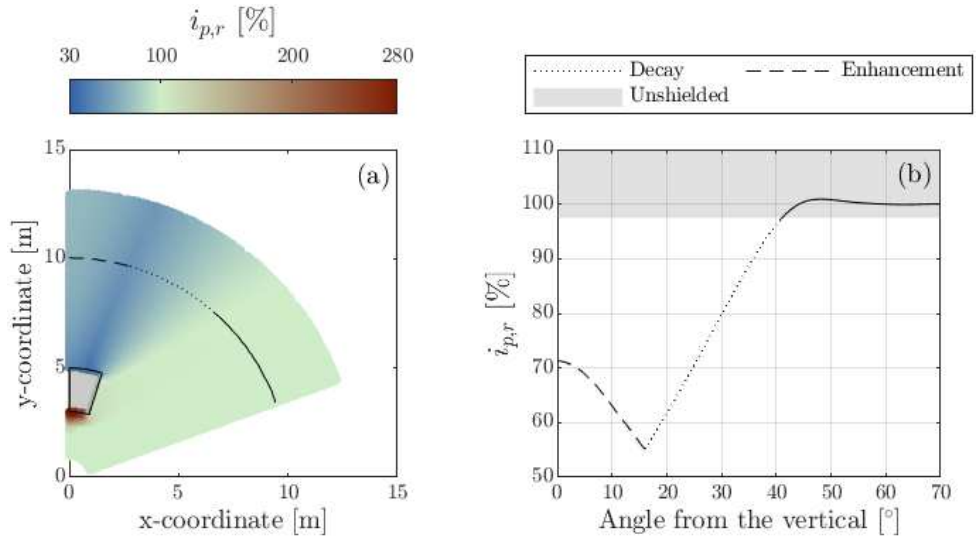

Figure 3: Spatial distribution of relative peak specific impulse for a representative obstacle (R= 5 m, θ= 35°, d = 2 m). (a) Plan elevation, with the charge positioned at the origin, and the obstacle is indicated by the grey block; and (b) Circumferential distribution at a constant radial distance.

4 DATA INTERROGATION AND INSIGHTS

4.1 Behaviours in the shielded region

Using Fig. 3(b), it is apparent that it is dichotomised between two regimes, termed ‘decay’ and ‘enhancement’. These are physically rationalised as follows.

Consider the blast wave as it propagates perfectly incidentally and one-dimensionally (besides some amount of interference from the reflecting face) alongside the obstacle. At the rear corner, the rigid obstacle is replaced by atmospheric air, resulting in a pressure differential that drives the otherwise radially propagating blast wave to expand circumferentially into the obstacle’s shadow. This loads the region above atmospheric conditions, but relatively less than had the obstacle not been present. As the shock travels deeper into the shadow, the loading lessens with increasing distance [17]. It is this process that rationalises the initial decay of the shielded region (depicted in Fig. 3(b), as the angle from the vertical reduces from 40° to 30°). Note, this expansion induces a rarefaction that propagates outwards from the obstacle into the otherwise free-field loading conditions, extending the load reduction effects beyond the obstacle’s immediate shadow.

As the shock continues to diffract circumferentially, it reaches a distinct minimum value in measured impulse (17° from the vertical in Fig. 3(b)). Thereafter, the loading increases due to superposition with the wave that diffracted around the opposite side of the obstacle. The effect of this interference is demonstrably maximal along the wall’s centreline, where the travelled distance for both waves is least, and their loading period is aligned. The subsequent wave, which propagates in the opposite direction to the first, excites points that have already been loaded, enhancing the measured peak impulse. As the interfering wave travels out from the centreline, not only does it continue to expand, but it arrives later and later through the first wave’s loading period. Ultimately its impulse enhancement lessens until it ceases to exceed the peak of the primary wave’s positive phase, hence the peak impulse in the decay region is unaffected by the superposition.

4.2 Behavioural consistency

The decay–enhancement dichotomy previously described arises exclusively and without exception for all 273 configurations simulated. Fig. 4 demonstrates this consistency in the behaviour of the shielded region. Depicted is the $i_{p,r}$ distribution as before (now with unshielded data eliminated), but for obstacles whose geometry is at the approximate upper and lower quartiles of the range of variable values considered in this investigation.

Whilst there are differences in the magnitudes of the relative peak specific impulse values across this range of problems, the pattern formed by the distribution of the loading is identical: a decay from the unshielded boundary to some minimum, followed by a rise to some maximum at the obstacle’s centreline. This behavioural pattern is also true at all radial distances behind an obstacle, as demonstrated in Fig. 5. At small distances behind the wall, the decay is exaggerated further by vortex shedding [13].

Ultimately, this consistency is a product of the generalised planar shock assumption being compelled in all instances. No other behaviours can physically arise because secondary behaviours are eliminated, and the self-similarity of the blast–obstacle interaction ensures that the primary behaviours always arise in the same way.

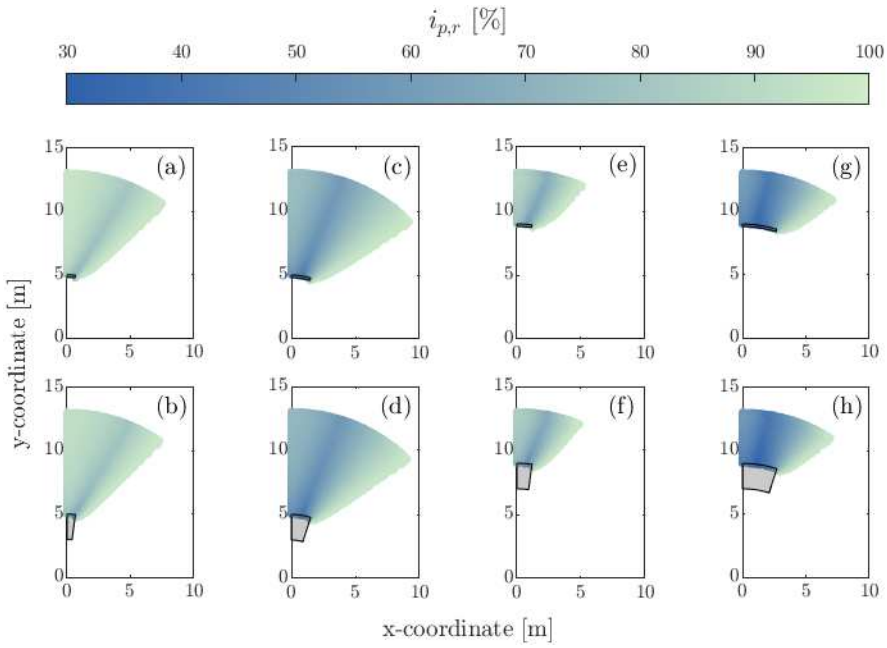

Figure 4: Spatial distribution of relative peak specific impulse in the shielded region of several obstacles. The obstacles are represented by the grey blocks, and the charge is positioned at the origin in all cases. (a) R = 5 m, θ = 15°, d = 0.2 m; (b) R = 5 m, θ = 15°, d = 2 m; (c) R = 5 m, θ = 35°, d = 0.2 m; (d) R = 5 m, θ = 35°, d = 2 m; (e) R = 9 m, θ = 15°, d = 0.2 m; (f) R = 9 m, θ = 15°, d = 2 m; (g) R = 9 m, θ = 35°, d = 0.2 m; (h) R = 9 m, θ = 35°, d =2 m.

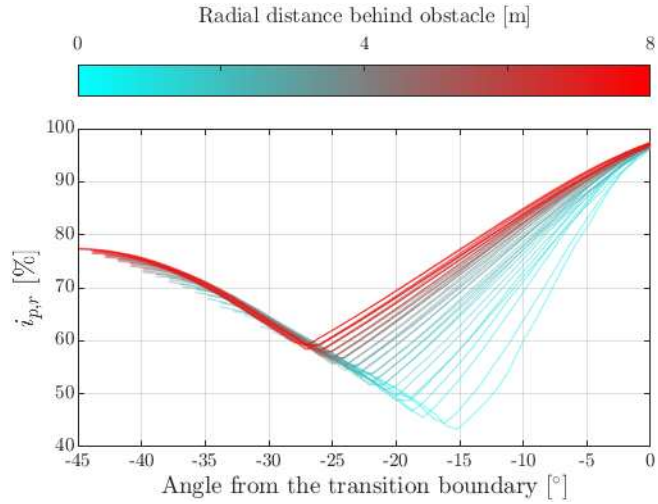

Figure 5: Circumferential distribution of relative peak specific impulse, plotted at each radial distance behind a representative obstacle (R = 5 m, θ = 35°, d = 0.2 m).

5 SELF-SIMILARITY AND PREDICTABILITY

5.1 An exploitable pattern

For several obstacles of differing geometry, Fig. 6 isolates and plots the spatial position of the transition boundary that delineates the shielded and unshielded regions. In all instances arc angle is variable whilst the obstacles' stand-off distance is constant (6 m). In Fig. 6(a), the obstacle depth is also constant (0.2 m), and it is qualitatively apparent that despite a variable arc angle, the transition boundary for all seven obstacles is approximately coincident.

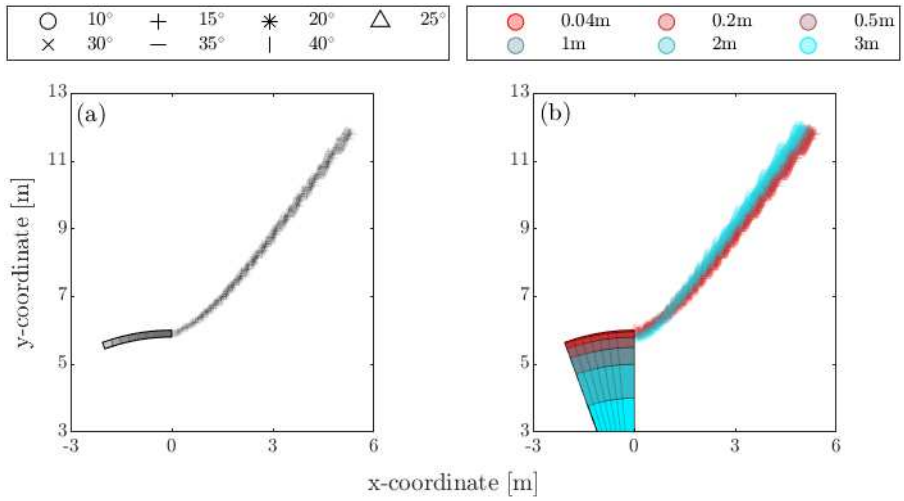

Figure 6: The spatial position of the shielded–unshielded transition boundaries of several obstacles. R = 6 m in all cases. (a) Obstacle θ is varied and d constant; and (b) Both θ and d are varied.

This is a consequence of two phenomena previously discussed. Firstly, the transition boundary is in the decay region beyond the minimum stream of measured peak impulse. The peak value of specific impulse at points in this region is exclusively the product of the primary wave; superposition with the mirrored diffracting shock is irrelevant here. Secondly, the initial conditions of the primary shock at the instant it begins to diffract around the rear corner of the obstacle are a function only of the stand-off distance (due to approximately one-dimensional incident propagation alongside the obstacle) and the obstacle's depth (which affects interference from the front face reflection). As such, the pressure differentials and momentum vectors that drive flow in the shielded region are identical for all these obstacles, given their common R and d. The impulse–time histories at the transition boundary are therefore identical in all these cases, diverging only upon the commencement of superposition (which occurs physically later or earlier depending on arc angle), by which time the peak value has already been reached.

Fig. 6(b) permits both arc angle and obstacle depth to vary (though only a single marker style is needed because the transition boundary has proven nominally independent of θ). It is shown that varying depth alters the spatial position of the transition boundary somewhat. However, considering that the depth has been varied by two orders of magnitude, the change

in the transition boundary's position is extremely small relatively, especially given that minor variability is to be expected having used a Cartesian mesh for this radial analysis [12]. This indicates another nominal independency (a conclusion supported by previous work [8]).

The transition boundary is simply the limiting case of the decay region. Consequently, the loading at all locations between the points of minimum impulse and the unshielded transition boundary must, by definition, be nominally independent of θ and d. Fig. 7(a) confirms this to be true, plotting the circumferential distribution of $i_{p,r}$ at a constant radial distance for the same array of obstacles as in Fig. 6(b).

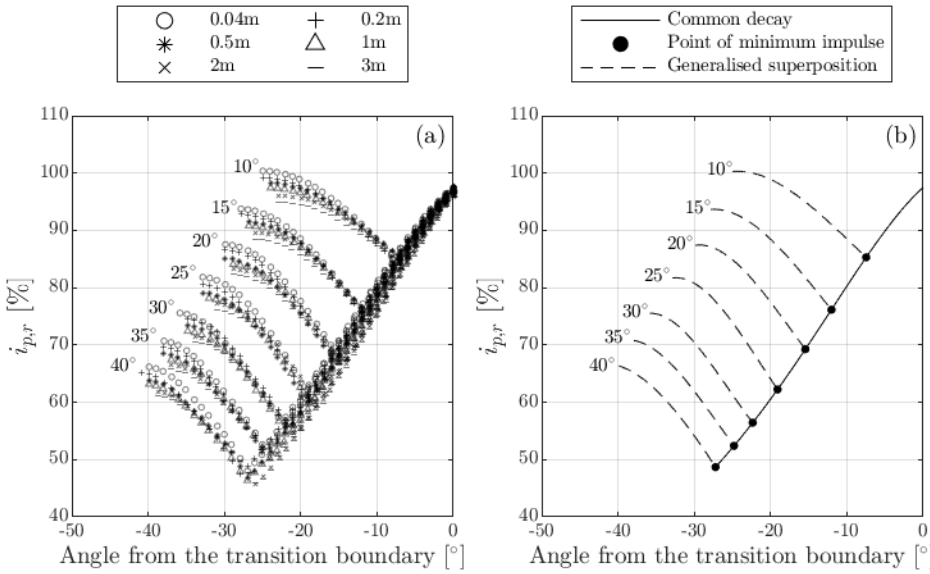

Figure 7: Circumferential distribution of relative peak specific impulse at a constant radial distance for obstacles of a constant R (6 m) and varied θ and d. (a) Raw data; and (b) Reduced-order representation.

5.2 A framework for prediction

Fig. 7(a) demonstrates that obstacles of differing arc angle and depth share a very similar decay from their transition boundary to their respective minimum, which has been physically rationalised. Branching from this common decay regime is the enhancement of impulse due to superposition. For obstacles of differing lateral extent, θ, the superposition occurs physically later or earlier, though this point of inflection occurs at approximately the same location for obstacles with the same lateral extent. Finally, though the superposition demonstrates some sensitivity to d, it is conservative in all instances to assume the obstacle to be infinitely thin.

From these observations, a reduced-order model of the impulse distribution within the shielded region can be constructed. Fig. 7(b) depicts this.

The behavioural consistency that has been demonstrated throughout this work means that the general form of this simplified model (though not its explicit magnitudes) describes the circumferential distribution of peak specific impulse at any stand-off distance in the shielded region of an annular sector obstacle of any geometry. Furthermore, because all secondary

interferences were eliminated, this pattern of behaviour represents the blast–obstacle interaction behaviour that is shielding, fundamentally and in isolation. Understanding and predicting the features highlighted in Fig. 7(b) would therefore be foundational to a fast-running engineering model (FREM) for the prediction of blast wave shielding that is generalisable and extensible to any scenario.

Direct polynomial assembly (e.g., [8], [9]) seems appropriate for said predictor, given the apparent simplicity of the decay profile, though the considerable data acquired in this study would also support the application of machine learning (ML). ML has successfully been leveraged in the prediction of urban blast loading, e.g., [22], [24], [25], though, once trained, such a tool is often described as a 'black box'. Not only does this prevent the user from learning about any novel physical relationships the model may have identified, but also it means that the model may not be conforming to the physical laws that we know to be true of the real-life problem. Past work has shown that ML failed to identify physics as well understood and simple as impulse's monotonic decay with increasing distance (in free-field conditions) [26]. The ML predictor attained a 'significant performance premium' [26, p. 148] once the researcher directly implemented this physics, demonstrating that an engineer's understanding of the physics governing a problem continues to add considerable value to such analyses [27].

6 SUMMARY AND OUTLOOK

Shielding is a blast–obstacle interaction behaviour of significant practical interest. Despite extensive prior study, however, the full lateral extent of the mitigation has yet to be mapped and reliably predicted. This work therefore extends prior parametric studies, exploring the relationship between an obstacle's dimensions and the shielding in its wake. 273 unique obstacle configurations were trialled in *Viper::Blast*, capturing the full lateral extent of their mitigation, as well as the magnitude and distribution of peak specific impulse within it. Critically, rather than a more typical rectilinear form, the obstacles employed in this study were annular sectors; by matching the curvature of the spherically expanding shock, all secondary interferences that may superpose with the shielding were eliminated, permitting its directed and isolated study.

The regime of behaviours within the shielded region was demonstrated to be consistent for obstacles of any size, scale, and stand-off distance. Several physically rationalised consequences of this self-similarity were identified, particularly that the decay in impulse during the diffraction into an obstacle's shadow was nominally independent of its lateral extent and its depth. From these principles, a simplified, physics-informed representation of the impulse distribution in an obstacle's shielded region was derived. Given the elimination of all secondary behaviours, this model is representative of shielding in isolation and therefore as a fundamental blast–obstacle interaction behaviour. Notably, this reduced-order model could form the basis for a framework for predicting the loading distribution within the wake of any obstacle, extensible beyond annular sectors.

A machine learning predictor for shielding could begin to be trained from the data acquired in this work. Furthermore, the direct interrogation and manipulation of the data identified several simple physical relationships that could be used to support its training. Yet, upon reflection, it is striking that had machine learning been applied without this critical appraisal of the data, several unique and elegant manifestations of the physics may never have been noticed, appreciated, and understood by the authors. They would instead have been lost within its black box, if it ever identified them at all.

ACKNOWLEDGEMENTS

J.K. would like to thank Baldan Devecioğlu for her assistance with the drawing package used to create some of the figures in this paper, and Dr. Dain G. Farrimond and Ross Waddoups for their formative insights. This work was performed as part of an iCASE PhD studentship funded by EPSRC and Synthetik Applied Technologies.

REFERENCES

[1] Smith, P.D., Rose, T.A. & Ng, S.H., The influence of areal density on the shielding and channelling of blast by buildings. *Proceedings of the Eighteenth International Symposium on Military Aspects of Blast and Shock*, 2004.

[2] Isaac, O.S., Alshammari, O.G., Pickering, E.G., Clarke, S.D. & Rigby, S.E., Blast wave interaction with structures: An overview. *International Journal of Protective Structures*, **14**(4), pp. 584–630, 2023. https://doi.org/10.1177/20414196221118595.

[3] Beyer, M.E., Blast loads behind vertical walls. *Proceedings of the 22nd Department of Defense Explosives Safety Seminar*, pp. 767–797, 1986.

[4] Rose, T.A., Smith, P.D. & Mays, G.C., Design charts relating to protection of structures against airblast from high explosives. *Proceedings of the Institution of Civil Engineers – Structures and Buildings*, **122**(2), pp. 186–192, 1997. https://doi.org/10.1680/istbu.1997.29307.

[5] Geng, J. & Thomas, J.K., Diffracted blast loads behind structures. *Proceedings of the ASME 2020 Pressure Vessels and Piping Conference*, pp. V004T04A008-1–V004T04A008-7, 2020.

[6] Gautier, A., Sochet, I. & Lapebie, E., Analysis of 3D interaction of a blast wave with a finite wall. *Shock Waves*, **32**(3), pp. 273–282, 2022. https://doi.org/10.1007/s00193-022-01081-7.

[7] Chapman, T.C., Rose, T.A. & Smith, P.D., Reflected blast wave resultants behind cantilever walls: A new prediction technique. *International Journal of Impact Engineering*, **16**(3), pp. 397–403, 1995. https://doi.org/10.1016/0734-743X(94)00051-W.

[8] Zhou, X.Q. & Hao, H., Prediction of airblast loads on structures behind a protective barrier. *International Journal of Impact Engineering*, **35**(5), pp. 363–375, 2008. https://doi.org/10.1016/j.ijimpeng.2007.03.003.

[9] Sung, S.-H. & Chong, J.-W., A fast-running method for blast load prediction shielding by a protective barrier. *Defence Technology*, **16**(2), pp. 308–315, 2020. https://doi.org/10.1016/j.dt.2019.07.011.

[10] United States Department of Defense, Structures to resist the effects of accidental explosions, UFC-3-340-02, United Facilities Criteria: Washington D.C., USA, 2008.

[11] Karlsen, J., Farrimond, D.G., Lodge, T.J., Rigby, S.E., Tyas, A., Clarke, S.D. & Brewer, T.R., Trilateration of blast wave arrival time: An inverse method for determining explosive yield and position. *Philosophical Transactions of the Royal Society A: Mathematical, Physical and Engineering Sciences*, in press.

[12] Payne, T., Williams, A., Worfolk, T. & Rigby, S., Numerical investigation into the influence of cubicle positioning in large-scale explosive arena trials. *International Journal of Protective Structures*, **7**(4), pp. 547–560, 2016. https://doi.org/10.1177/2041419616676438.

[13] Norris, C.H., Hansen, R.J., Myle, J.H. Jr., Biggs, J.M., Namyet, S. & Minami, J.K., *Structural Design for Dynamic Loads*, 1st ed., McGraw-Hill: New York, USA, 1959.

[14] Beshara, F.B.A., Modelling of blast loading on aboveground structures: I. General phenomenology and external blast. *Computers and Structures*, **51**(5), pp. 585–596, 1994. https://doi.org/10.1016/0045-7949(94)90066-3.
[15] Glasstone, S. & Dolan, P.J., *The Effects of Nuclear Weapons*, 3rd ed., United States Department of Defense; Energy Research and Development Administration: Washington D.C., USA, 1977.
[16] United States Department of Homeland Security. IED attack fact sheet: Improvised explosive devices. https://www.dhs.gov/publication/ied-attack-fact-sheet. Accessed on: 17 Apr. 2023.
[17] Taylor, G.I., The formation of a blast wave by a very intense explosion I. Theoretical discussion. *Proceedings of the Royal Society of London. Series A. Mathematical and Physical Sciences*, **201**(1065), pp. 159–174, 1950. https://doi.org/10.1098/rspa.1950.0049.
[18] Ben-Dor, G., *Shock Wave Reflection Phenomena*, 2nd ed., Springer: Berlin, Germany, 2007.
[19] Needham, C.E., *Blast Waves*, 1st ed., Springer: Berlin, Germany, 2010.
[20] Farrimond, D.G., Rigby, S.E., Clarke, S.D. & Tyas, A., Time of arrival as a diagnostic for far-field high explosive blast waves. *International Journal of Protective Structures*, **13**(2), pp. 379–402, 2022. https://doi.org/10.1177/20414196211062923.
[21] Stirling, G.C., *Viper::Blast User Manual and Examples for Version 1.20.0*, Stirling Simulation Services Limited: Glasgow, UK, 2021.
[22] Dennis, A.A. & Rigby, S.E., The direction-encoded neural network: A machine learning approach to rapidly predict blast loading in obstructed environments. *International Journal of Protective Structures*, **15**(3), pp. 455–483, 2024. https://doi.org/10.1177/20414196231177364.
[23] Chester, A., Hazael, R. & Critchley, R., Comparative analysis of blast prediction software for far-field shock wave effects behind a blast wall. *International Journal of Protective Structures*, **0**(0), pp. 1–28, 2024. https://doi.org/10.1177/20414196241284299.
[24] Dennis, A. & Rigby, S., Prediction of blast loads using machine learning approaches. *Proceedings of the 2023 Society for Earthquake and Civil Engineering Dynamics Conference*, 2023.
[25] Dennis, A.A., A direction-encoded machine learning approach for peak overpressure prediction in urban environments. *Proceedings of the Nineteenth International Symposium on Interaction of the Effects of Munitions with Structures*, 2024.
[26] Pannell, J.J., Surrogate modelling strategies for the prediction of near-field blast impulse. PhD thesis, University of Sheffield, 2022.
[27] Karlsen, J. & Rigby, S.E., The role of AI in engineering: Towards rapid inverse blast analysis. *Proceedings of the Fourth International Conference on Structural Safety Under Fire & Blast Loading*, 2024.